



Sulfate formation via aerosol phase SO₂ oxidation by model biomass burning photosensitizers: 3,4-dimethoxybenzaldehyde, vanillin and syringaldehyde using single particle characterization

Liyuan Zhou^{1,2}, Zhancong Liang^{1,2}, Brix Raphael Go^{1,2}, Rosemarie Ann Infante Cuevas^{1,2},
Rongzhi Tang^{1,2}, Mei Li^{3,4}, Chunlei Cheng^{3,4} and Chak K. Chan^{1,2,5*}

¹School of Energy and Environment, City University of Hong Kong, Hong Kong, China

²City University of Hong Kong Shenzhen Research Institute, Shenzhen, China

³Institute of Mass Spectrometry and Atmospheric Environment, Guangdong Provincial Engineering Research Center for On-line Source Apportionment System of Air Pollution, Jinan University, Guangzhou 510632, China

⁴Guangdong-Hongkong-Macau Joint Laboratory of Collaborative Innovation for Environmental Quality, Guangzhou 510632, China

⁵Low-Carbon and Climate Impact Research Centre of School of Energy and Environment, City University of Hong Kong, Hong Kong, China

Correspondence to: Chak K. Chan (Chak.K.Chan@cityu.edu.hk)



Abstract. Atmospheric oxidation of sulfur dioxide (SO_2) to sulfate has been widely investigated by means of gas phase and in-cloud chemistry studies. Recent field measurements have shown significant sulfate formation in cloud-free environments with high aerosol loadings. As an important fraction of biomass burning aerosol components, particulate phenolic and non-phenolic aromatic carbonyls may initiate photosensitized aerosol multiphase oxidation of SO_2 , of which our knowledge however is still in its nascent stage. In this study, on the basis of single-particle aerosol mass spectrometry (SPAMS) measurements, we find evident sulfate formation in the biomass burning-derived photosensitizer particles under UV and SO_2 exposure, attributable to photosensitized oxidation of S(IV) , while almost no sulfate was observed under dark and existence of SO_2 . The efficiency of sulfate production under UV irradiation, represented by the number percentage of sulfate-containing particles (99-43%) and sulfate relative peak area (RPA) (0.67-0.12) in single particle spectra, in descending order, were 3,4-dimethoxybenzaldehyde (DMB), vanillin (VL) and syringaldehyde (SyrAld). Internal mixtures of VL and potassium nitrate gave a slightly lower number percentage and RPA of sulfate to VL particles alone. In externally mixed potassium nitrate and VL particles, sulfate was predominantly formed on the latter, confirming that sulfate formation via photosensitization prevails over that via nitrate photolysis. Our results suggest that photosensitized oxidation of S(IV) could make an important contribution to aerosol sulfate formation, especially in areas influenced by biomass burning.

1. Introduction

Sulfate is a key component of fine particulate matter in the atmosphere, which impacts air quality, climate, and human and ecosystem health (Nel, 2005; Fuzzi et al., 2015; Grantz et al., 2003). Traditional atmospheric models, including the gas-phase oxidation of sulfur dioxide (SO_2) by hydroxyl radical (OH) (Calvert et al., 1978) and stabilized Criegee intermediates (Cheng et al., 2016) and a series of aqueous, in-cloud oxidation of SO_2 , underpredict the sulfate production during heavy pollution episodes in China (Zheng et al., 2015; Zhang et al., 2015; Wang et al., 2014; Liu and Abbatt, 2021). Although the liquid water content (LWC) is generally much lower in aerosol particles than in fog and cloud droplets, it was reported that aerosol multiphase oxidation processes are important, especially in polluted and high relative humidity (RH) conditions (Liu et al., 2021; Liu et al., 2020). The typical oxidants involved in multiphase oxidation of S(IV) in aerosol particles include dissolved ozone (O_3) (Hoffmann and Calvert, 1985), hydrogen peroxide (H_2O_2) (Hoffmann and Calvert, 1985), transition metal ions



(TMIs, i.e., Fe (III) and Mn(II)) (Ibusuki and Takeuchi, 1987; Harris et al., 2013; Alexander et al., 2009; Martin and Good, 1991), methyl hydrogen peroxide (Walcek and Taylor, 1986) and peroxyacetic acid (Walcek and Taylor, 1986). To narrow the gap between the measured and modeled sulfate production, new chemical pathways have been suggested involving nitrogen dioxide (NO_2) (Wang et al., 2016; Cheng et al., 2016), organic peroxides (Yao et al., 2019; Ye et al., 2018), oxidants from particulate nitrate photolysis (Gen et al., 2019b, a; Zhang et al., 2020), and hypohalous acid (HOX, e.g., HOCl and HOBr) (Liu and Abbatt, 2020). However, the missing sulfate source has still remained unclear and controversial.

Photosensitization in atmospheric aerosols has been recently proposed to initiate novel chemistry in the formation of secondary pollutants (George et al., 2015). Upon irradiation, atmospheric photosensitizers such as aromatic carbonyls can generate triplet excited states ($^3\text{C}^*$) (Canonica et al., 1995; Anastasio et al., 1996; Smith et al., 2014; Kaur and Anastasio, 2018; Kaur et al., 2019; Smith et al., 2016), which can oxidize phenols at higher rates compared to OH, particularly under acidic conditions (Smith et al., 2014). In addition to being an oxidant, $^3\text{C}^*$ can also react with O_2 to generate secondary oxidants, such as singlet oxygen ($^1\text{O}_2$), superoxide (O_2^-), hydroperoxyl radical ($^{\bullet}\text{HO}_2$), and $^{\bullet}\text{OH}$ (Corral Arroyo et al., 2018; Dalrymple et al., 2010; George et al., 2018). Biomass burning is an important source of aromatic carbonyls (Rogge et al., 1998; Nolte et al., 2001; Schauer et al., 2001), and the concentrations of phenolic and non-phenolic carbonyls are comparable in biomass burning smoke (Simoneit et al., 1993; Anastasio et al., 1996). Direct photosensitized oxidation of vanillin (a typical aromatic carbonyl photosensitizer) has been reported as an important pathway to form aqueous secondary organic aerosol in areas influenced by biomass burning, with reaction products dominated by brown carbon chromophores (Mabato et al., 2022b; Mabato et al., 2022a). However, only limited studies focused on the role of biomass burning-derived photosensitizers in S(IV) oxidation (Wang et al., 2020; Wang et al., 2021). In this study, we investigate sulfate formation via aerosol phase SO_2 oxidation by biomass burning-derived photosensitizers, including both non-phenolic (3,4-dimethoxybenzaldehyde, DMB) and phenolic photosensitizers (vanillin, VL and syringaldehyde, SyrAld) with similar molar absorptivity at atmospheric relevant wavelengths (Figure S1, Supporting information), in an oxidation flow reactor (OFR) utilizing a single particle aerosol mass spectrometer (SPAMS). Nitrate photolysis has been reported as a typical sulfate formation pathway initiated by particulate photoactive compounds, similar to photosensitization (Gen et al., 2022). The objectives of this study are to semi-quantitatively



evaluate the extent of sulfate formation in photosensitizer particles and qualitatively compare the relative atmospheric importance of particulate photosensitization and nitrate photolysis in sulfate formation.

2. Methods

2.1 Materials and experimental setup

A vaporization - condensation method was used to coat photosensitizing or non-photosensitizing species on 0.3 μm polystyrene latex sphere (PSL) particles (Thermo Fisher Scientific Inc., MA) (Qi et al., 2019). A detailed experimental setup is shown in Figure S2a and the initial experimental conditions are summarized in Table S1. All chemicals, including DMB (Acros Organics, 99+%), VL (Acros Organics, 99%), SyrAld (Sigma Aldrich, 98%), benzoic acid (BA, Acros Organics, 99.6%), potassium nitrate (KNO_3 , Sigma Aldrich, 99+%) and oxalic acid (Sigma Aldrich, 99.9+%) were used as purchased. PSL particles were selected as condensation nuclei due to their chemically and thermally inert nature. Their size did not change upon passing through the dryer or glass bottle at 120°C oil bath or exposure to SO_2 or UV irradiation (Figure S3). In addition, PSL particles are difficult to be ionized and do not complicate the interpretation of mass spectra. PSL condensation nuclei were generated by using a constant output atomizer (TSI 3076) with pure N_2 gas (>99.995 %), and a portion of the particles passed through a diffusion dryer at a flow rate of 300 mL min^{-1} to achieve $\text{RH} < 10\%$. The dried particles subsequently passed through a heated glass bottle (inlet about 2 inches above the bottom) containing ~0.5g of either DMB, VL, SyrAld or BA at the bottom. The heating temperatures of the glass bottle were regulated using an oil bath near the melting points of the chemicals. The generated organic vapor condensed to form coatings onto the PSL particles. The coating thickness was estimated by the measured particle size increase by the SPAMS. For control experiments with PSL-only particles, the particles passed through the same glass bottle containing no chemicals. Photosensitizing (DMB, VL, SyrAld) (Smith et al., 2015, 2016; Smith et al., 2014) and non-photosensitizing (BA) (Smith et al., 2015) species coated particles or uncoated PSL-only particles were then introduced into an OFR (volume of approximately 7.2 L) and mixed with SO_2 gas. SO_2 was delivered by a flow of around 11 mL min^{-1} (203 ppm, mixing with pure N_2 , Scientific Gas Engineering Co., Ltd.) to achieve the SO_2 concentration of around 750 ppb in the OFR. Depending on the experiment, the RH in the OFR was regulated at ~80% or 20% by passing HEPA-filtered and activated-carbon-denuded compressed air or pure N_2 through water bubblers. Experiments under air enable



the generation of secondary oxidants. Conversely, the N_2 experiments would inhibit the formation of secondary oxidants, which can lead to triplets-driven reactions (Chen et al., 2020). The total flow in the OFR was around 3 L min^{-1} , resulting in a residence time of $\sim 2.5 \text{ min}$. There are four UVA lamps (Shenzhen Guanhongrui Technology Co., Ltd.) with a continuous emission spectrum over 310–420 nm surrounding the OFR. We conducted experiments with one and four lamps to provide a total irradiance of about $1.1 \times 10^{15} \text{ (I}_1\text{)}$ and $3.8 \times 10^{15} \text{ (I}_4\text{)}$ $\text{photon cm}^{-2} \text{ s}^{-1}$, respectively (see details in Supporting information, Text S1); and dark control experiments were performed with UV lamps off. Each experiment lasted around 20 minutes. In the absence of light and SO_2 , there was no change in the mass spectra of coated particles (Figure S4). At the outlet of the OFR, SO_2 concentration was monitored by a SO_2 analyzer (Teledyne, T100, USA), and the size and chemical composition of individual aerosol particles were analyzed by a single particle aerosol mass spectrometry (SPAMS, Hexin Analytical Instrument Co., Ltd, China). This single particle technique allows us to study the mixing state of the particles. KNO_3 was widely observed in biomass burning plumes (Zauscher et al., 2013). Internally mixed particles of photosensitizing species and KNO_3 were generated by atomizing aqueous solutions of KNO_3 with several drops of PSL suspension, followed by passing through a dryer and then the heated glass bottle containing photosensitizing species as described above (Figure S2a). Externally mixed particles were generated with a second atomizer (TSI 9032), and the generated KNO_3 or KNO_3 -oxalic acid mixed particles were mixed with photosensitizing species coated particles in a stainless-steel chamber ($\phi 3 \times 8''$) before introduction to the OFR (Figure S2b).

2.2 SPAMS and data analysis

A detailed description of the operational principle of SPAMS has been provided elsewhere (Li et al., 2011). Briefly, aerosol particles were introduced into the SPAMS through an orifice and aerodynamic lens and consecutively irradiated by two laser beams, where their aerodynamic diameter were determined through the velocity and flight time. The sized particles were then desorbed and ionized by a pulsed 266 nm laser (0.5 mJ), which was triggered at the precise time on the basis of the particle velocities. The produced positive and negative molecular fragments were analyzed by a Z-shaped bipolar time-of-flight mass spectrometer (Pratt et al., 2009; Li et al., 2011). The single particle size and mass spectral analysis were performed using the Computational Continuation Core (COCO) toolkit based on MATLAB software. The number percentage and relative peak



area (RPA, defined as the fractional contribution of the targeted ion peak area to the sum of all ion peak areas) were applied to indicate the variations of different species (e.g., sulfate) in individual particles (Hu et al., 2022). Sulfate-containing particles were distinguished by m/z -97 [HSO_4^-] or m/z -96 [SO_4^-] (Guazzotti et al., 2001; Liang et al., 2022). In addition, an adaptive resonance theory based neural network algorithm (ART-2a) (Li et al., 2011) was used to separate and cluster particles in external and internal mixtures according to the similarities in individual mass spectra of single particles.

3. Results and discussion

Figure 1a shows the changes in SO_2 concentration ($[\text{SO}_2]$) in the presence of PSL particles coated with various types of photosensitizing (DMB, VL and SyrAld) and non-photosensitizing (BA) species under dark and UV irradiation conditions. In Figure 1a, for UV condition, only time traces of SO_2 under I_4 UV irradiance were shown for clarity, and I_1 UV irradiance cases can be found in Figure S5. Except stated otherwise, results shown in the following discussions were obtained at 80% RH. The steady concentration of SO_2 in the OFR was at around 750 ppb under dark conditions. Upon exposure to UV light, a rapid drop in the SO_2 concentration was observed in the presence of DMB- and VL-coated particles, indicating photoinduced uptake of SO_2 on these particles. A recent study suggests that the photosensitized chemical reactions between naphthalene-derived secondary organic aerosol and SO_2 likely occur at the particle surface (Wang et al., 2021). In this study, the SO_2 consumption under UV irradiation for DMB and VL coated particles increased with the surface area of SPAMS detected particles in the OFR (Figure 1a and S6) ($R^2=0.84-0.99$). Total surface area concentrations in the range of 7×10^4 - $2 \times 10^5 \mu\text{m}^2 \text{m}^{-3}$ are denoted by “small”, in 2×10^5 - $6 \times 10^5 \mu\text{m}^2 \text{m}^{-3}$ as “medium”, and larger than $6 \times 10^5 \mu\text{m}^2 \text{m}^{-3}$ as “large”. These values fall within the urban background and indoor air ranges but are slightly lower than urban pollution ranges (Willeke and Whitby, 1975; Hudda and Fruin, 2016; Qi et al., 2008). SO_2 consumption per unit surface area concentration also increased with higher UV irradiance (Figure S6). Only slight SO_2 consumption under UV irradiation was observed in the presence of SyrAld-coated particles and no observable decrease in SO_2 concentrations in the absence of photosensitizing species, i.e., BA-coated particles and PSL-only particles. The average mass spectra of DMB-, VL-, SyrAld- and BA-coated single particles under dark and UV irradiation in the presence of SO_2 are shown in Figure 1b, characterized by their respective parent ions (in either neutral, protonated or deprotonated form) and expected smaller organic fragment ions. PSL-only particles do not ionize and no mass spectra were



observed (Qi et al., 2019). No sulfate was formed under dark condition, consistent with the stable SO_2 concentrations observed. However, upon exposure to UV irradiation, the RPA of sulfate ($^{97}\text{HSO}_4^-$ and $^{96}\text{SO}_4^-$) increased significantly, accompanied by the slight decrease of RPA of the parent ions of $^{165}\text{C}_9\text{H}_9\text{O}_3^{+/-}$, $^{153}\text{C}_8\text{H}_9\text{O}_3^{+/-}$, $^{181}\text{C}_9\text{H}_9\text{O}_4^{+/-}$ for DMB-, VL- and SyrAld-coated particles respectively. Figure 2 shows a considerable difference in the average RPA of sulfate (circles) and the number percentage of sulfate-containing particles (diamonds) in DMB-, VL-, SyrAld- and BA-coated particles at dark and different UV intensities in the presence of SO_2 , and the corresponding SO_2 consumption normalized by the average total particle surface area concentration before and after UV irradiation in the OFR detected by SPAMS (crosses). The average number percentages of sulfate-containing particles in DMB- and VL- coated particles are considerably higher ($> 84\%$) under both I_1 and I_4 UV irradiances than under dark ($< 2\%$). SyrAld-coated particles gave a slightly lower percentage of sulfate-containing particles of 43% and 83% at I_1 and I_4 UV irradiances. Upon increase of photon flux densities (I_1 to I_4), the RPA of sulfate increases for DMB-, VL- and SyrAld-coated particles, which is in line with the enhanced normalized SO_2 consumptions.

The loss of SO_2 associated with the synchronous sulfate production in single DMB-, VL- and to a lesser extent, SyrAld-coated particles was likely attributed to the photosensitization-induced oxidation of S(IV) (i.e., SO_2 , HSO_3^- , and SO_3^{2-}). Specifically, UV irradiation could excite photosensitizers from their ground state to singlet excited state, then rapidly relax to a triplet state via intersystem crossing (George et al., 2015; Gomez Alvarez et al., 2012). S(IV) could be oxidized to sulfate directly by $^3\text{C}^*$, or by the secondary oxidants (e.g., $^1\text{O}_2$, $\text{O}_2^{\bullet-}/\text{HO}_2$ and $^{\bullet}\text{OH}$) produced from the excited molecules and O_2/water . Wang et al. (2020) observed sulfate production from direct reactions between triplets of 4-(benzoyl) benzoic acid, humic acid and their salts, and hydrated S(IV).

In our previous study, we have reported the enhanced SO_2 oxidation and sulfate formation in incense and mosquito coil burning particles (Liang et al., 2022), as surrogates of biomass burning organic aerosol, BBOA (Li et al., 2012; Zhang et al., 2014), under light, compared with dark conditions. The number percentage of sulfate-containing particles increased from around 50% under dark to around 90% after UV irradiation (Figure 2). Incense burning particles contain a variety of photosensitizers, e.g., DMB, VL and SyrAld (Peng et al., 2020; Liu and Sun, 1988; Liang et al., 2022), which could oxidize SO_2 via photosensitization. In contrast to Liang et al. (2022), we did not observe sulfate formation under dark in the current



study. The much higher percentage of sulfate-containing particles under dark in incense burning particles in Liang et al. (2022) than in the photosensitizer particles in this study was likely due to the gaseous oxidants in incense-burning plumes. Furthermore, as mentioned earlier, in the control experiment using BA-coated particles as seeds in the presence of SO₂, neither the RPA of sulfate nor the number percentage of sulfate-containing particles changed upon irradiation. This indicates that the direct photoexcitation of SO₂ in the presence of water leading to the formation of OH and subsequently sulfate plays a negligible role (Kroll et al., 2018; Martins-Costa et al., 2018; Wang et al., 2021). Although the coating thickness estimated by particle size increase spanned a wide range from 100 nm to 2.2 μm, the number percentage and RPA of sulfate generally exhibited the similar descending order of DMB>VL>SyrAld>BA in each size bin (Figure S7). Interestingly, our observed trend of sulfate formation potential is in line with the secondary organic aerosol mass yield for syringol oxidation by ³C* of DMB (114%), VL (111%) and SyrAld (78%) in the literature (Smith et al., 2016; Smith et al., 2014).

The triplet excited state (³C*) of aromatic carbonyls can react with O₂ in air-saturated conditions via either energy transfer to form ¹O₂ or electron transfer to form O₂^{•−}, which can further react with H⁺ ion to produce H₂O₂ and [•]OH (Dalrymple et al., 2010). Therefore, the absence of O₂ in N₂ saturated experiments would inhibit the formation of secondary oxidants. Figure 3 shows that replacing air by pure N₂ substantially shifted the distribution of RPA for DMB- and VL-coated particles toward the lower end, while SyrAld-coated particles exhibited slight changes. For example, DMB-coated particles with sulfate RPA larger than 0.6 were dominant and comprised more than 52% of total particles in air, but more than 73% of the total particles had sulfate RPA of 0-0.2 in N₂ under both UV irradiances. This suggests the involvement of O₂ and the potential important role of secondary oxidants in sulfate formation. Upon the increase of UV intensity (from I₁ to I₄), the number fraction of particles with sulfate RPA larger than 0.2 only slightly increased in N₂-saturated conditions, and particles with RPA of 0-0.2 dominated the population, indicating the relatively minor role of direct ³C* oxidation of SO₂. In contrast, Wang et al. (2020) reported that switching from air to N₂ resulted in similar S(IV) oxidation rates, indicating that the direct reaction of SO₂ with ³C* was more significant than that with the secondary oxidants. This discrepancy is possibly due to different reactivities of ³C* from different photosensitizing chemicals towards SO₂. In air, DMB-coated particles exhibited the strongest SO₂ oxidation potential with 88% of the total particles having sulfate RPA larger than 0.2 (I₁), followed by VL- (41%) and SyrAld- (15%) coated particles. Upon exposure to simulated sunlight, SyrAld and VL have been shown to undergo apparent direct



photodegradation, but DMB exhibits smaller or almost no loss in illuminated solution mixed with non-carbonyl phenols or benzene-diols (Smith et al., 2016, 2015; Smith et al., 2014). This is generally consistent with the decrease of RPA of parent ions in this study (Figure S8). The rapid direct photodegradation of phenolic carbonyls (VL and SyrAld) can reduce their concentrations in the particles and limits the formation of sulfate. Note that the photosensitizers may be (polymorphic) solid or semi-solid due to their low solubility and hygroscopicity (Kavuru et al., 2016; Hussain et al., 2001). For example, Mochida and Kawamura (2004) reported that pyrolysis products of lignin with -COOH, including vanillic acid and syringic acid, showed no hygroscopic growth even at RH of more than 90%. They also proposed that other pyrolysis products with chemical structures such as -CHO may have even lower hygroscopicity than -COOH and would not show measurable particle growth.

Nitrate is a ubiquitous constituent of atmospheric aerosol particles (Chan and Yao, 2008). Multiphase photochemical oxidation of SO₂ by the photolysis of particulate nitrate could make an important contribution to aerosol sulfate formation (Gen et al., 2019a, b). To qualitatively compare the relative atmospheric importance of photosensitization and nitrate photolysis in sulfate formation, external mixtures of VL-coated particles and KNO₃ particles were exposed to SO₂ and UV irradiation at 80% RH. VL was used for comparison owing to its moderate sulfate formation potential among the three photosensitizers tested. Potassium was the dominant cation in biomass burning plumes (Jahn et al., 2021; Frenay et al., 2009), and therefore KNO₃ was selected as the model nitrate salt. RPA of sulfate for VL-coated particles and KNO₃ particles at different sizes in the external mixture were compared in Figure 4a. VL-coated particles exhibited an average sulfate RPA of 0.26, with an overall inverse relationship with particle size, while the sulfate absolute peak areas (APA) are moderately higher for large particles. The APA is proportional to the absolute number of ions detected and a larger sulfate APA may indicate a larger amount of sulfate formed. However, APA is more sensitive to the variability in ion intensities associated with particle-laser interactions than RPA (Gross et al., 2000; Hatch et al., 2014). The reactive uptake comprises the diffusion of SO₂ molecules, followed by oxidation of SO₂ at the interface or in the bulk of the particles. The decreased sulfate RPA with increasing particle size may be attributed to the photosensitized sulfate formation at the surface of VL-coated particles or diffusional limitations of SO₂ in larger particles, especially in the poorly hygroscopic and potentially viscous VL matrix. In contrast, deliquescent KNO₃ particles (Figure S9) exhibited RPAs of 0, suggesting that nitrate photolysis plays a negligible role in our study, although the concentration of [NO₃⁻] in KNO₃ particles at 80% RH was estimated to be 6.3 M by AIOMFAC



(<http://www.aiomfac.caltech.edu>) (Zuend et al., 2008), almost 100 times higher than the solubility of VL (~66 mM). The prevailing sulfate formation in VL particles over KNO_3 particles is likely due to the lower integrated molar absorptivity of nitrate ($\sim 143 \text{ M}^{-1} \text{ cm}^{-1}$) compared to VL ($2.8 \times 10^5 \text{ M}^{-1} \text{ cm}^{-1}$) over the wavelength range of 300–400 nm (Figure S1). In addition, this also excluded the possibility of sulfate formation in gas phase and small nuclei, which would be expected to have condensed/coagulated on both the photosensitizer and KNO_3 particles. When RH decreased to 20%, a significant reduction in the average RPAs from 0.26 to 0.002 was observed for VL-coated particles (Figure S10). This may be due to the fewer dissolved VL for sulfate formation. Overall, sulfate formation was found on VL-coated particles but not on externally mixed nitrate particles. Oxalic acid is one of the most abundant species of organic aerosols and is commonly found in atmospheric nitrate-containing particles (Mochizuki et al., 2017; Cheng et al., 2017; Yang et al., 2009). We have also conducted experiments with internal mixtures of KNO_3 and oxalic acid, which did not show sulfate formation as well (Figure 4b). However, internally mixed VL and KNO_3 yielded 55% sulfate-containing particles and an average sulfate RPA of 0.12. These values fall in between those of pure KNO_3 and VL-coated particles (Figure 4c). As the ion intensity ratio of nitrate to organics of the KNO_3 -VL internally mixed particles of similar size decreased, higher sulfate RPAs were found.

4. Environmental implications

This paper presents insights on aerosol SO_2 oxidation by biomass burning-derived photosensitizers using single particle characterization. Sulfate formation in photosensitizer coated particles, in terms of both number percentage and RPA of sulfate, was significantly higher under UV irradiation than under dark. From dark to UV irradiation, the average number percentages of sulfate-containing particles increased from less than 2% to 43–99%, and sulfate RPA increased from almost 0 to 0.12–0.67 for SyrAld, VL, and DMB-coated particles.

The speciation, concentration, and properties of photosensitizers in ambient particles are still poorly understood, limiting the parameterization of photosensitized sulfate formation. Nevertheless, we observed that sulfate formation via photosensitization is qualitatively more efficient than nitrate photolysis. Recently, we found that incense burning particles



(considered as typical BBOA surrogates) show increases of sulfate-containing particles and sulfate RPAs by ~45% and ~0.35 under UV than dark, respectively, due to photosensitization reactions of SO₂ (Liang et al., 2022). These results are within the ranges of our measurements in this paper. The SO₂ exposure of ~1800 ppb min in the OFR in this study corresponds to a 45 min and 450 min atmospheric SO₂ exposure, taking an ambient RH of 80% and SO₂ concentration of 40 ppb during extreme haze events (Cheng et al., 2016) and 4 ppb in usual days (Chen et al., 2022), respectively. This indicates that after exposure of tens of minutes to hours to SO₂, more than 40% of fresh BBOA particles could contain sulfate via photosensitization, especially under high photon flux such as during typical clear days and haze days in Beijing, China, which were around 4 and 1.4 times, respectively, of that in the OFR (I₄) (Figure S1). Our finding provides additional experimental support to the potentially important contribution of photosensitized oxidation of S(IV) to aerosol sulfate formation in biomass burning plumes. Future studies of the quantification and mechanism revelation of sulfate formation via photosensitization are needed. In addition, we solely studied three typical biomass burning-derived photosensitizers. Photosensitized sulfate formation on real BBOA particles, which is a complex matrix of organics, is to be explored further.

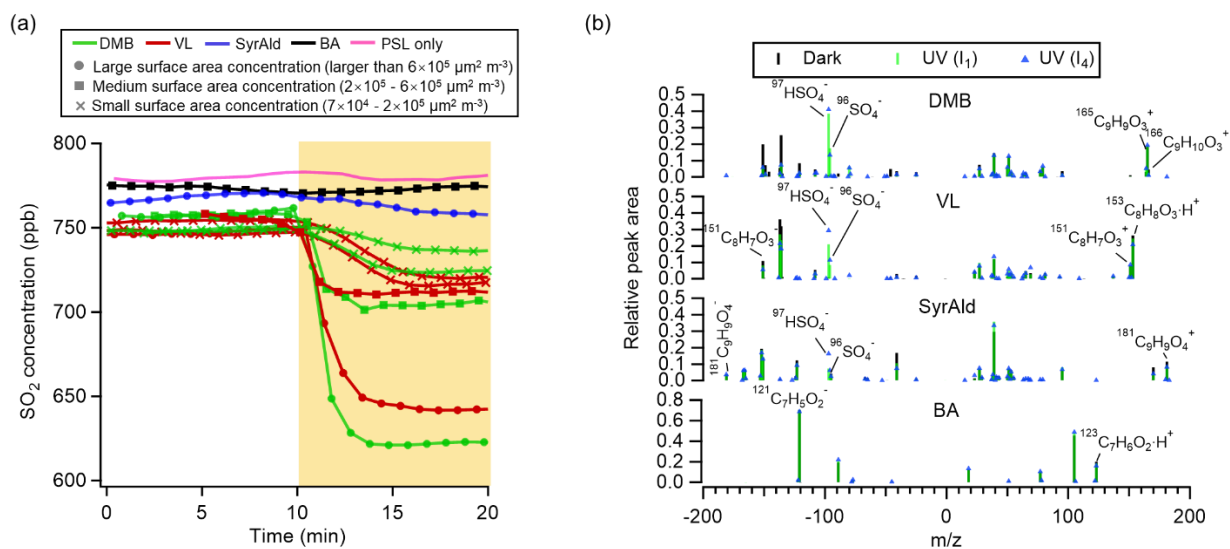


Figure 1. (a) Time traces of SO_2 in the dark (0–10 min) and under UV irradiation (I_4) (10–20 min) in the presence of DMB-, VL-, SyrAld-, or BA-coated particles and PSL-only particles. The SO_2 consumption is presented as a function of the total surface area concentration of SPAMS detected particles. Total surface area concentrations in the range of $7 \times 10^4 - 2 \times 10^5 \mu\text{m}^2 \text{m}^{-3}$ are denoted by “small”, in $2 \times 10^5 - 6 \times 10^5 \mu\text{m}^2 \text{m}^{-3}$ as “medium”, and larger than $6 \times 10^5 \mu\text{m}^2 \text{m}^{-3}$ as “large”. (b) Average negative and positive mass spectra for the DMB-, VL-, SyrAld- and BA-coated particles under dark and UV irradiation (I_1 and I_4) conditions. All experiments were conducted at 80% RH.

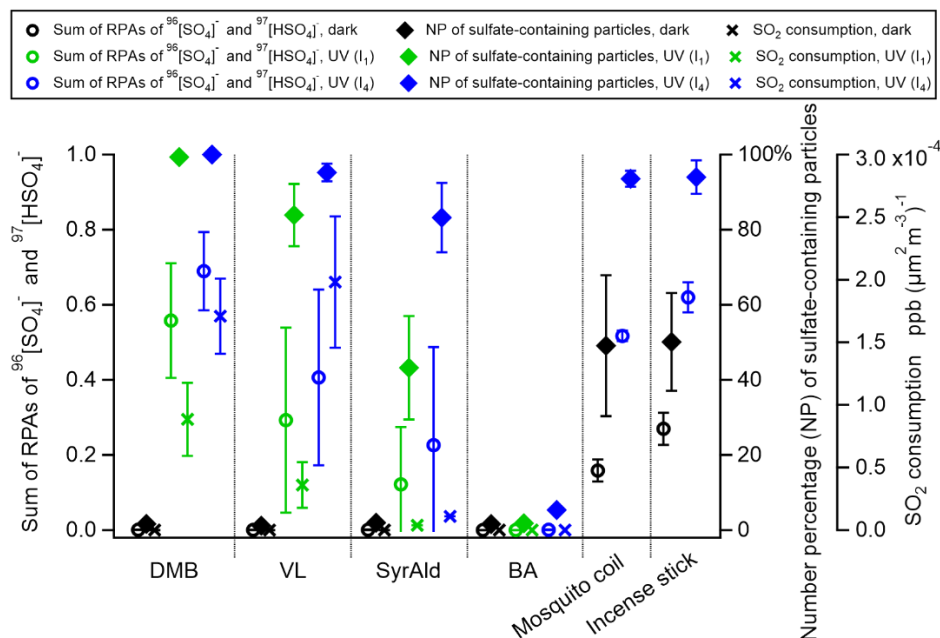


Figure 2. Average sulfate relative peak areas (RPAs), and number percentage of sulfate-containing particles for the DMB-, VL-, SyrAld- and BA-coated particles, mosquito coil burning, and incense burning particles under dark and UV irradiation conditions in the presence of SO_2 . Errors are shown by 95% confidence intervals. SO_2 consumptions normalized by the average total particle surface area concentrations before and after UV irradiation in the OFR detected by SPAMS are shown. Data of incense and mosquito coil burning particles were from Liang et al. (2022). All experiments were conducted at 80% RH.

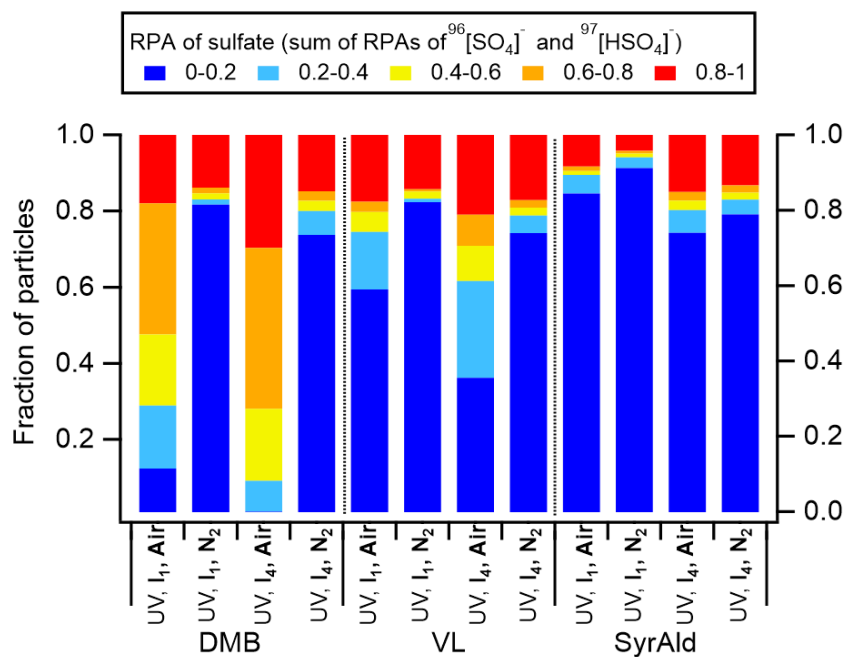


Figure 3. Distribution of sulfate RPA for DMB-, VL- and SyrAld-coated particles under air and N₂ conditions at different UV intensities in the presence of SO₂.

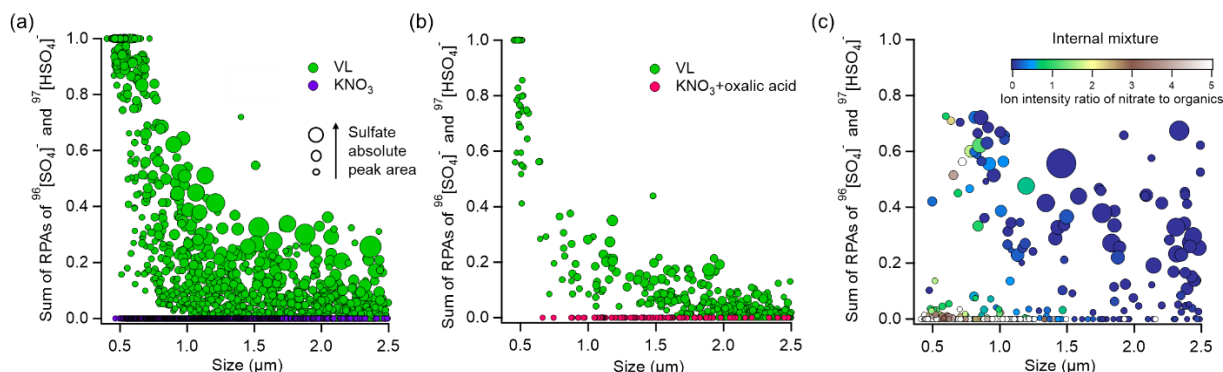


Figure 4. Sulfate RPA vs. particle diameter detected by the SPAMS for (a) externally mixed VL-coated particles and KNO_3 ; (b) externally mixed VL-coated particles and KNO_3 -oxalic acid particles; and (c) internally mixed VL and KNO_3 particles at 80% RH under UV irradiation (I_1) in the presence of SO_2 . The markers are presented as a function of sulfate APA. The color scale in c indicates the ion intensity ratio of nitrate to organics (total negative ion intensity subtracted by nitrate and sulfate intensity) in the negative mass spectra.

Data availability. The data are available upon request to the corresponding author.

Author contributions. CKC and LZ designed the experiment; LZ and ZL conducted the experiments; LZ and ZL performed the data interpretation; LZ, ZL, BRG, RAIC, RT, ML, CC and CKC wrote the paper. All authors contributed to the paper with useful scientific discussions or comments.

Competing interests. The contact author has declared that neither they nor their co-authors have any competing interests.

Acknowledgements. We gratefully acknowledge the support from the Hong Kong Research Grants Council (No.11304121, R1016-20F) and the National Natural Science Foundation of China (No. 42275104).



References

- Alexander, B., Park, R. J., Jacob, D. J., and Gong, S.: Transition metal-catalyzed oxidation of atmospheric sulfur: Global implications for the sulfur budget, *Journal of Geophysical Research: Atmospheres*, 114, 2009.
- Anastasio, C., Faust, B. C., and Rao, C. J.: Aromatic carbonyl compounds as aqueous-phase photochemical sources of hydrogen peroxide in acidic sulfate aerosols, fogs, and clouds. 1. Non-phenolic methoxybenzaldehydes and methoxyacetophenones with reductants (phenols), *Environmental science & technology*, 31, 218-232, 1996.
- Calvert, J. G., BOTTENHEIM, J. W., and STRAUSZ, O. P.: Mechanism of the homogeneous oxidation of sulfur dioxide in the troposphere, in: *Sulfur in the Atmosphere*, Elsevier, 197-226, 1978.
- Canonica, S., Jans, U., Stemmler, K., and Hoigne, J.: Transformation kinetics of phenols in water: photosensitization by dissolved natural organic material and aromatic ketones, *Environmental science & technology*, 29, 1822-1831, 1995.
- Chan, C. K., and Yao, X.: Air pollution in mega cities in China, *Atmospheric environment*, 42, 1-42, 2008.
- Chen, C.-H., Tsai, C.-Y., Chen, T.-F., Hou, L.-S., and Chang, K.-H.: Temporal Trends and Spatial Distribution Characteristics of Air Quality Monitored in China from 2015 to 2020, *Journal of Innovative Technology*, 4, 23-28, 2022.
- Chen, Y., Li, N., Li, X., Tao, Y., Luo, S., Zhao, Z., Ma, S., Huang, H., Chen, Y., and Ye, Z.: Secondary organic aerosol formation from 3C*-initiated oxidation of 4-ethylguaiaicol in atmospheric aqueous-phase, *Science of The Total Environment*, 723, 137953, 2020.
- Cheng, C., Li, M., Chan, C. K., Tong, H., Chen, C., Chen, D., Wu, D., Li, L., Wu, C., and Cheng, P.: Mixing state of oxalic acid containing particles in the rural area of Pearl River Delta, China: implications for the formation mechanism of oxalic acid, *Atmospheric Chemistry and Physics*, 17, 9519-9533, 2017.
- Cheng, Y., Zheng, G., Wei, C., Mu, Q., Zheng, B., Wang, Z., Gao, M., Zhang, Q., He, K., and Carmichael, G.: Reactive nitrogen chemistry in aerosol water as a source of sulfate during haze events in China, *Science advances*, 2, e1601530, 2016.
- Corral Arroyo, P., Bartels-Rausch, T., Alpert, P. A., Dumas, S. p., Perrier, S. b., George, C., and Ammann, M.: Particle-phase photosensitized radical production and aerosol aging, *Environmental science & technology*, 52, 7680-7688, 2018.
- Dalrymple, R. M., Carfagno, A. K., and Sharpless, C. M.: Correlations between dissolved organic matter optical properties and quantum yields of singlet oxygen and hydrogen peroxide, *Environmental science & technology*, 44, 5824-5829, 2010.
- Frenay, E. J., Martin, S. T., and Buseck, P. R.: Deliquescence and efflorescence of potassium salts relevant to biomass-burning aerosol particles, *Aerosol Science and Technology*, 43, 799-807, 2009.
- Fuzzi, S., Baltensperger, U., Carslaw, K., Decesari, S., Denier van der Gon, H., Facchini, M. C., Fowler, D., Koren, I., Langford, B., and Lohmann, U.: Particulate matter, air quality and climate: lessons learned and future needs, *Atmospheric chemistry and physics*, 15, 8217-8299, 2015.
- Gen, M., Zhang, R., Huang, D. D., Li, Y., and Chan, C. K.: Heterogeneous oxidation of SO₂ in sulfate production during nitrate photolysis at 300 nm: effect of pH, relative humidity, irradiation intensity, and the presence of organic compounds, *Environmental Science & Technology*, 53, 8757-8766, 2019a.
- Gen, M., Zhang, R., Huang, D. D., Li, Y., and Chan, C. K.: Heterogeneous SO₂ oxidation in sulfate formation by photolysis of particulate nitrate, *Environmental Science & Technology Letters*, 6, 86-91, 2019b.



- 328 Gen, M., Liang, Z., Zhang, R., Mabato, B. R. G., and Chan, C. K.: Particulate nitrate photolysis in the atmosphere,
 329 Environmental Science: Atmospheres, 2022.
- 330 George, C., Ammann, M., D'Anna, B., Donaldson, D., and Nizkorodov, S. A.: Heterogeneous photochemistry in the
 331 atmosphere, Chemical reviews, 115, 4218-4258, 2015.
- 332 George, C., Brüggemann, M., Hayeck, N., Tinel, L., and Donaldson, J.: Interfacial Photochemistry, in: Physical Chemistry of
 333 Gas-Liquid Interfaces, Elsevier, 435-457, 2018.
- 334 Grantz, D., Garner, J., and Johnson, D.: Ecological effects of particulate matter, Environment international, 29, 213-239, 2003.
- 335 Gross, D. S., Gälli, M. E., Silva, P. J., and Prather, K. A.: Relative sensitivity factors for alkali metal and ammonium cations
 336 in single-particle aerosol time-of-flight mass spectra, Analytical Chemistry, 72, 416-422, 2000.
- 337 Guazzotti, S. A., Coffee, K. R., and Prather, K. A.: Continuous measurements of size-resolved particle chemistry during
 338 INDOEX-Intensive Field Phase 99, Journal of Geophysical Research: Atmospheres, 106, 28607-28627, 2001.
- 339 Harris, E., Sinha, B., Van Pinxteren, D., Tilgner, A., Fomba, K. W., Schneider, J., Roth, A., Gnauk, T., Fahlbusch, B., and
 340 Mertes, S.: Enhanced role of transition metal ion catalysis during in-cloud oxidation of SO₂, Science, 340, 727-730, 2013.
- 341 Hatch, L. E., Pratt, K. A., Huffman, J. A., Jimenez, J. L., and Prather, K. A.: Impacts of aerosol aging on laser
 342 desorption/ionization in single-particle mass spectrometers, Aerosol Science and Technology, 48, 1050-1058, 2014.
- 343 Hoffmann, M. R., and Calvert, J. G.: Chemical Transformation Modules for Eulerian Acid Deposition Models: Volume II, the
 344 Aqueous-phase Chemistry., EPA/600/3-85, 17, 1985.
- 345 Hu, X., Guo, Z., Sun, W., Lian, X., Fu, Y., Meng, H., Zhu, Y., Zhang, G., Wang, X., and Xue, L.: Atmospheric Processing of
 346 Particulate Imidazole Compounds Driven by Photochemistry, Environmental Science & Technology Letters, 9, 265-271, 2022.
- 347 Hudda, N., and Fruin, S.: International airport impacts to air quality: size and related properties of large increases in ultrafine
 348 particle number concentrations, Environmental science & technology, 50, 3362-3370, 2016.
- 349 Hussain, K., Thorsen, G., and Malthe-Sørensen, D.: Nucleation and metastability in crystallization of vanillin and ethyl
 350 vanillin, Chemical engineering science, 56, 2295-2304, 2001.
- 351 Ibusuki, T., and Takeuchi, K.: Sulfur dioxide oxidation by oxygen catalyzed by mixtures of manganese (II) and iron (III) in
 352 aqueous solutions at environmental reaction conditions, Atmospheric Environment (1967), 21, 1555-1560, 1987.
- 353 Jahn, L. G., Jahl, L. G., Bowers, B. B., and Sullivan, R. C.: Morphology of organic carbon coatings on biomass-burning
 354 particles and their role in reactive gas uptake, ACS Earth and Space Chemistry, 5, 2184-2195, 2021.
- 355 Kaur, R., and Anastasio, C.: First measurements of organic triplet excited states in atmospheric waters, Environmental science
 356 & technology, 52, 5218-5226, 2018.
- 357 Kaur, R., Labins, J. R., Helbock, S. S., Jiang, W., Bein, K. J., Zhang, Q., and Anastasio, C.: Photooxidants from brown carbon
 358 and other chromophores in illuminated particle extracts, Atmospheric Chemistry and Physics, 19, 6579-6594, 2019.
- 359 Kavuru, P., Grebinoski, S. J., Patel, M. A., Wojtas, L., and Chadwick, K.: Polymorphism of vanillin revisited: the discovery
 360 and selective crystallization of a rare crystal structure, CrystEngComm, 18, 1118-1122, 2016.
- 361 Kroll, J. A., Frandsen, B. N., Kjaergaard, H. G., and Vaida, V.: Atmospheric hydroxyl radical source: Reaction of triplet SO₂
 362 and water, The Journal of Physical Chemistry A, 122, 4465-4469, 2018.



- 363 Li, L., Huang, Z., Dong, J., Li, M., Gao, W., Nian, H., Fu, Z., Zhang, G., Bi, X., and Cheng, P.: Real time bipolar time-of-
 364 flight mass spectrometer for analyzing single aerosol particles, *International Journal of Mass Spectrometry*, 303, 118-124,
 365 2011.
- 366 Li, Y. J., Yeung, J. W., Leung, T. P., Lau, A. P., and Chan, C. K.: Characterization of organic particles from incense burning
 367 using an aerodyne high-resolution time-of-flight aerosol mass spectrometer, *Aerosol science and technology*, 46, 654-665,
 368 2012.
- 369 Liang, Z., Zhou, L., Infante Cuevas, R. A., Li, X., Cheng, C., Li, M., Tang, R., Zhang, R., Lee, P. K., and Lai, A. C.: Sulfate
 370 Formation in Incense Burning Particles: A Single-Particle Mass Spectrometric Study, *Environmental Science & Technology*
 371 *Letters*, 2022.
- 372 Liu, T., and Abbatt, J. P.: An experimental assessment of the importance of S (IV) oxidation by hypohalous acids in the marine
 373 atmosphere, *Geophysical Research Letters*, 47, e2019GL086465, 2020.
- 374 Liu, T., Clegg, S. L., and Abbatt, J. P.: Fast oxidation of sulfur dioxide by hydrogen peroxide in deliquesced aerosol particles,
 375 *Proceedings of the National Academy of Sciences*, 117, 1354-1359, 2020.
- 376 Liu, T., and Abbatt, J. P.: Oxidation of sulfur dioxide by nitrogen dioxide accelerated at the interface of deliquesced aerosol
 377 particles, *Nature Chemistry*, 13, 1173-1177, 2021.
- 378 Liu, T., Chan, A. W., and Abbatt, J. P.: Multiphase oxidation of sulfur dioxide in aerosol particles: implications for sulfate
 379 formation in polluted environments, *Environmental Science & Technology*, 55, 4227-4242, 2021.
- 380 Liu, W., and Sun, S.: Ultrastructural changes of tracheal epithelium and alveolar macrophages of rats exposed to mosquito coil
 381 smoke, *Toxicology letters*, 41, 145-157, 1988.
- 382 Mabato, B. R. G., Li, Y. J., Huang, D. D., Wang, Y., and Chan, C. K.: Aqueous SOA formation from photosensitized guaiacol
 383 oxidation: Comparison between non-phenolic and phenolic methoxybenzaldehydes as photosensitizers in the absence and
 384 presence of ammonium nitrate, *Atmospheric Chemistry and Physics Discussions*, 1-25, 2022a.
- 385 Mabato, B. R. G., Lyu, Y., Ji, Y., Li, Y. J., Huang, D. D., Li, X., Nah, T., Lam, C. H., and Chan, C. K.: Aqueous secondary
 386 organic aerosol formation from the direct photosensitized oxidation of vanillin in the absence and presence of ammonium
 387 nitrate, *Atmospheric Chemistry and Physics*, 22, 273-293, 2022b.
- 388 Martin, L. R., and Good, T. W.: Catalyzed oxidation of sulfur dioxide in solution: The iron-manganese synergism, *Atmospheric*
 389 *Environment. Part A. General Topics*, 25, 2395-2399, 1991.
- 390 Martins-Costa, M. T., Anglada, J. M., Francisco, J. S., and Ruiz-López, M. F.: Photochemistry of SO₂ at the air–water
 391 interface: a source of OH and HOSO radicals, *Journal of the American Chemical Society*, 140, 12341-12344, 2018.
- 392 Mochida, M., and Kawamura, K.: Hygroscopic properties of levoglucosan and related organic compounds characteristic to
 393 biomass burning aerosol particles, *Journal of Geophysical Research: Atmospheres*, 109, 2004.
- 394 Mochizuki, T., Kawamura, K., Miyazaki, Y., Wada, R., Takahashi, Y., Saigusa, N., and Tani, A.: Secondary formation of
 395 oxalic acid and related organic species from biogenic sources in a larch forest at the northern slope of Mt. Fuji, *Atmospheric*
 396 *environment*, 166, 255-262, 2017.
- 397 Nel, A.: Air pollution-related illness: effects of particles, *Science*, 308, 804-806, 2005.
- 398 Nolte, C. G., Schauer, J. J., Cass, G. R., and Simoneit, B. R.: Highly polar organic compounds present in wood smoke and in
 399 the ambient atmosphere, *Environmental science & technology*, 35, 1912-1919, 2001.



- 400 Peng, D.-Q., Yu, Z.-X., Wang, C.-H., Gong, B., Liu, Y.-Y., and Wei, J.-H.: Chemical Constituents and Anti-Inflammatory
 401 Effect of Incense Smoke from Agarwood Determined by GC-MS, *International Journal of Analytical Chemistry*, 2020, 2020.
- 402 Pratt, K. A., Mayer, J. E., Holecek, J. C., Moffet, R. C., Sanchez, R. O., Rebotier, T. P., Furutani, H., Gonin, M., Fuhrer, K.,
 403 and Su, Y.: Development and characterization of an aircraft aerosol time-of-flight mass spectrometer, *Analytical chemistry*,
 404 81, 1792-1800, 2009.
- 405 Qi, C., Stanley, N., Pui, D. Y., and Kuehn, T. H.: Laboratory and on-road evaluations of cabin air filters using number and
 406 surface area concentration monitors, *Environmental science & technology*, 42, 4128-4132, 2008.
- 407 Qi, X., Pang, X., Hong, Y., Wang, Y., Lou, S., Feng, J., Cheng, P., and Zhou, Z.: Real-time analysis of the homogeneous and
 408 heterogeneous reactions of pyrene with ozone by SPAMS and CRD-EAS, *Chemosphere*, 234, 608-617, 2019.
- 409 Rogge, W. F., Hildemann, L. M., Mazurek, M. A., Cass, G. R., and Simoneit, B. R.: Sources of fine organic aerosol. 9. Pine,
 410 oak, and synthetic log combustion in residential fireplaces, *Environmental Science & Technology*, 32, 13-22, 1998.
- 411 Schauer, J. J., Kleeman, M. J., Cass, G. R., and Simoneit, B. R.: Measurement of emissions from air pollution sources. 3. C1–
 412 C29 organic compounds from fireplace combustion of wood, *Environmental science & technology*, 35, 1716-1728, 2001.
- 413 Simoneit, B. R., Rogge, W., Mazurek, M., Standley, L., Hildemann, L., and Cass, G.: Lignin pyrolysis products, lignans, and
 414 resin acids as specific tracers of plant classes in emissions from biomass combustion, *Environmental science & technology*,
 415 27, 2533-2541, 1993.
- 416 Smith, J. D., Sio, V., Yu, L., Zhang, Q., and Anastasio, C.: Secondary organic aerosol production from aqueous reactions of
 417 atmospheric phenols with an organic triplet excited state, *Environmental science & technology*, 48, 1049-1057, 2014.
- 418 Smith, J. D., Kinney, H., and Anastasio, C.: Aqueous benzene-diols react with an organic triplet excited state and hydroxyl
 419 radical to form secondary organic aerosol, *Physical Chemistry Chemical Physics*, 17, 10227-10237, 2015.
- 420 Smith, J. D., Kinney, H., and Anastasio, C.: Phenolic carbonyls undergo rapid aqueous photodegradation to form low-volatility,
 421 light-absorbing products, *Atmospheric Environment*, 126, 36-44, 2016.
- 422 Walcek, C. J., and Taylor, G. R.: A theoretical method for computing vertical distributions of acidity and sulfate production
 423 within cumulus clouds, *Journal of Atmospheric Sciences*, 43, 339-355, 1986.
- 424 Wang, G., Zhang, R., Gomez, M. E., Yang, L., Levy Zamora, M., Hu, M., Lin, Y., Peng, J., Guo, S., and Meng, J.: Persistent
 425 sulfate formation from London Fog to Chinese haze, *Proceedings of the National Academy of Sciences*, 113, 13630-13635,
 426 2016.
- 427 Wang, X., Gemayel, R., Hayeck, N., Perrier, S., Charbonnel, N., Xu, C., Chen, H., Zhu, C., Zhang, L., and Wang, L.:
 428 Atmospheric photosensitization: a new pathway for sulfate formation, *Environmental Science & Technology*, 54, 3114-3120,
 429 2020.
- 430 Wang, X., Gemayel, R., Baboian, V. J., Li, K., Boreave, A., Dubois, C., Tomaz, S., Perrier, S., Nizkorodov, S. A., and
 431 George, C.: Naphthalene-Derived Secondary Organic Aerosols Interfacial Photosensitizing Properties, *Geophysical Research*
 432 *Letters*, 48, e2021GL093465, 2021.
- 433 Wang, Y., Zhang, Q., Jiang, J., Zhou, W., Wang, B., He, K., Duan, F., Zhang, Q., Philip, S., and Xie, Y.: Enhanced sulfate
 434 formation during China's severe winter haze episode in January 2013 missing from current models, *Journal of Geophysical*
 435 *Research: Atmospheres*, 119, 10,425-410,440, 2014.



- 436 Willeke, K., and Whitby, K. T.: Atmospheric aerosols: size distribution interpretation, Journal of the Air Pollution Control
437 Association, 25, 529-534, 1975.
- 438 Yang, F., Chen, H., Wang, X., Yang, X., Du, J., and Chen, J.: Single particle mass spectrometry of oxalic acid in ambient
439 aerosols in Shanghai: Mixing state and formation mechanism, Atmospheric Environment, 43, 3876-3882, 2009.
- 440 Yao, M., Zhao, Y., Hu, M., Huang, D., Wang, Y., Yu, J. Z., and Yan, N.: Multiphase reactions between secondary organic
441 aerosol and sulfur dioxide: kinetics and contributions to sulfate formation and aerosol aging, Environmental Science &
442 Technology Letters, 6, 768-774, 2019.
- 443 Ye, J., Abbatt, J. P., and Chan, A. W.: Novel pathway of SO₂ oxidation in the atmosphere: reactions with monoterpene
444 ozonolysis intermediates and secondary organic aerosol, Atmospheric Chemistry and Physics, 18, 5549-5565, 2018.
- 445 Zauscher, M. D., Wang, Y., Moore, M. J., Gaston, C. J., and Prather, K. A.: Air quality impact and physicochemical aging of
446 biomass burning aerosols during the 2007 San Diego wildfires, Environmental science & technology, 47, 7633-7643, 2013.
- 447 Zhang, R., Wang, G., Guo, S., Zamora, M. L., Ying, Q., Lin, Y., Wang, W., Hu, M., and Wang, Y.: Formation of urban fine
448 particulate matter, Chemical reviews, 115, 3803-3855, 2015.
- 449 Zhang, R., Gen, M., Huang, D., Li, Y., and Chan, C. K.: Enhanced sulfate production by nitrate photolysis in the presence of
450 halide ions in atmospheric particles, Environmental Science & Technology, 54, 3831-3839, 2020.
- 451 Zhang, Y., Zhang, X., Sun, J., Hu, G., Shen, X., Wang, Y., Wang, T., Wang, D., and Zhao, Y.: Chemical composition and
452 mass size distribution of PM₁ at an elevated site in central east China, Atmospheric Chemistry and Physics, 14, 12237-12249,
453 2014.
- 454 Zheng, B., Zhang, Q., Zhang, Y., He, K., Wang, K., Zheng, G., Duan, F., Ma, Y., and Kimoto, T.: Heterogeneous chemistry:
455 a mechanism missing in current models to explain secondary inorganic aerosol formation during the January 2013 haze episode
456 in North China, Atmospheric Chemistry and Physics, 15, 2031-2049, 2015.
- 457 Zuend, A., Marcolli, C., Luo, B. P., and Peter, T.: A thermodynamic model of mixed organic-inorganic aerosols to predict
458 activity coefficients, Atmospheric Chemistry and Physics, 8, 4559-4593, 2008.
- 459